Optics Letters

Enhancing excited-state lifetimes in Er^{3+}-doped silica glass through controlled heat exposure

Tim Julian Wörmann,[1,*] Martin Brunzell,[1] Valdas Pasiskevicius,[1] and Pawel Maniewski[1,2]

[1]Department of Applied Physics, KTH Royal Institute of Technology, Hannes Alfvéns väg 12, 114 19 Stockholm, Sweden
[2]Optoelectronic Research Centre, University of Southampton, University Rd., Southampton SO17 1BJ, UK
*twormann@kth.se

Received 14 March 2025; revised 12 May 2025; accepted 19 May 2025; posted 19 May 2025; published 3 June 2025

Optimization of rare-earth (RE) doped devices for laser applications necessitates a combination of precision material engineering and advanced performance enhancement strategies. This study presents a novel investigation, to our knowledge, into cluster dynamics in Er-doped glass, utilizing localized CO_2 laser heating to simulate the high-temperature conditions typical of glass fabrication processes. Our findings demonstrate that, by a controlled heat exposure, it is possible to influence clustering in Er-doped glass. Minimized clustering leads to a significant improvement in material properties and ultimately device performance. Specifically, we achieved up to 25% increase in the radiative lifetime associated with the $^4I_{13/2} \rightarrow {}^4I_{15/2}$ radiative transition by exposing samples to elevated temperatures for several minutes. This rapid thermal treatment minimizes dopant mobility in sintered silica glass, thereby reducing cluster formation and improving the homogeneity of the active medium. These results provide a feasible pathway for enhancing the performance of erbium-based optical devices, including lasers and signal amplifiers, and underscore the potential of thermal processing as a versatile tool in photonic material optimization.

https://doi.org/10.1364/OL.562095

Rare-earth (RE)-doped materials exhibit significant potential across numerous optical applications such as solid-state optical devices, lasers, nonlinear optics, and optical fibers [1]. Their unique properties make them particularly valuable in the development of fiber lasers and amplifiers offering several advantages over traditional crystal or gas-based gain materials. RE-doped fiber lasers and amplifiers are favored for their variability of different active materials and fiber scaling to gain the desired high-power scaling and high-quality beams [2]. Commonly, RE-doped glasses used in fiber devices are made using modified chemical vapor deposition (MCVD) in combination with solution doping [3–5]. This multistep procedure that includes silica soot formation, soaking, drying, and collapsing is inherently linked to long exposure to high temperatures. To obtain high gain per waveguide length, it is favorable to attain high doping concentrations of RE ions [6]. On the one hand, high doping levels can reduce the length of active waveguides, thereby minimizing nonlinear effects such as self-phase modulation and stimulating Raman scattering [7,8]. On the other hand, high doping levels are challenging to obtain in silica due to relatively low solubility for RE ions. The latter is typically mitigated by co-doping with alumina (Al_2O_3) or phosphorus oxide (P_2O_5) [9]. Co-doping with alumina modifies the silica glass network by forming Al–O–Si bonds that are typically more accommodating for RE ions. In such compositions, it was shown that alumina doping prevents the RE ions from clustering that causes a well-documented concentration quenching. In RE ionic clusters, pump energy can be exchanged between two RE ions, leading to parasitic upconversion (UC) and cross-relaxation effects that have detrimental effects on the desired emission [10–12]. Besides precise control of material composition through multi-element doping, processing conditions i.e., the means of manufacturing, may significantly influence quenching dynamics. In general, long processing times at elevated temperatures increase dopant mobility, thereby enabling well-documented, undesired effects such as phase separation, diffusion, oxidation, and dissociation of elements [13,14]. For instance, thermal history and fabrication process were shown to have strong influence when doping with Tm^{3+}, Ho^{3+}, and Yb^{3+} [15,16]. On the contrary, erbium doping (Er^{3+}) has shown limited response to thermal post-processing. This suggests that the Er^{3+} clustering must be linked to faster interactions and thus early stage of manufacturing, which is more challenging to investigate when traditional, lengthy glassmaking techniques are used [15,17]. In recent years, RE-doped gain fibers have been made using few unconventional methods [18–21]. Primarily, laser-based methods enable the reduction of small-scale fiber fabrication time. This is due to the ability of lasers to provide rapid, localized, and time-intermittent heating. This controlled heat exposure also facilitates the investigation of early glass-formation stages, which play a critical role in cluster formation. To unveil dynamics linked to Er^{3+} cluster formation, we studied laser-sintered Er^{3+}-doped glass samples. To obtain the samples, powder mixture matching common concentrations of Er^{3+} [18,19] were laser-sintered directly on the end face of

a multi-mode fiber (MMF). The rapid laser sintering, which was used to obtain the samples, enables to evaluate early doping diffusion and ion interactions during glassmaking. In other words, this way of glass prototyping allows for low-cost process optimization without the need for lengthy try-and-error fiber optimization. This work shows that by careful optimization of manufacturing parameters and glass thermal history, it is possible to enhance the properties of Er^{3+}-doped optical fibers, although this method can readily be applied to other RE. By using lasers, glass melting temperatures can be obtained rapidly with steep heating and cooling rates. For silica, a CO_2 laser operating at $\lambda = 10.6\,\mu m$ is particularly suitable. At this wavelength, the beam penetration is only several microns, while the absorption of the beam leads to the rapid increase of temperature. Subsequently, the energy is conducted to underlying regions through heat conduction and radiation. Laser heating is often leveraged in glass shaping, fiber splicing, or post-processing [22]. Rapid, laser-aided melting can be also used in glassmaking, i.e., to melt and sinter powders and powder mixtures. Thus, it offers a feasible way to obtain the desired doping profiles [23].

Figure 1 depicts heat flow simulation (COMSOL Multiphysics) of a test sample used in this work. It is based on the heat balance equation in the time-dependent spatial frame, which balances variations of thermal energy by convection and thermal dependent emission of silica [24], thermal conduction, and additional heat sources (here in the form of the incident laser beam). The model of CO_2 laser-based heating was built similarly as it was described in [25]. For silica, the temperature dependent absorption coefficient ($\alpha(T)$) for $\lambda = 10.6\,\mu m$ was approximated by Eq. (1), based on the data available in [26]:

$$\alpha(T) = \frac{4\pi}{\lambda}(1.82 \cdot 10^{-2} + 10.1 \cdot 10^{-5} K^{-1}(T - 273.15K)). \quad (1)$$

In the simulation, the tip of the silica cylinder (diameter of 125 μm) was reaching an equilibrium temperature of approximately 2260 K (sufficient for glass softening). through CO_2 laser exposure (normal incidence, $\lambda = 10.6\,\mu m$, $P = 4\,W$ (spot size = 100 μm, Gaussian, as depicted in Fig. 1(a)), with comparable cooling rates, as shown Fig. 1(b). The laser-based approach provides highly controlled heat exposure to the fiber tip, enabling the evaluation of glass samples at various stages of processing.

To investigate the dynamics of cluster formation during the laser-based glass fabrication process, we developed a glass test sample that incorporated an Er^{3+} doping level of 0.7 wt%, which corresponds in its composition to the earlier reported fiber laser made through laser powder deposition [19]. The samples used in our experiments were laser-sintered glass *hemispheres* made directly on the end face of a commercial multi-mode fiber (LIEKKI Passive-105/125 DC). The use of MMF as the host for our glass samples helps with the collection of the excited emission. The fabrication procedure consisted of a few steps: First, a nano-powder mixture (see Table 1) was prepared. To obtain the mixture, the respective nano-powders, were measured by weight, suspended in methanol, and mixed until homogenous. The obtained suspension was air-dried, and then it was deposited by dip coating onto a cleaved end face of the MMF. Subsequently, a focused CO_2 laser pulse ($\lambda = 10.6\,\mu m$, $P = 4\,W$, $t = 0.5\,s$, $M^2 < 1.3$) was launched at the powder-covered tip of the fiber. The absorption of the laser beam melted the fiber tip, sintered the powders, and enabled a gradual diffusion of inter alia dopants into the glass matrix. The resultant rounded shape of the sample was determined by its surface tension and typically had a curvature radius of approximately 60 μm.

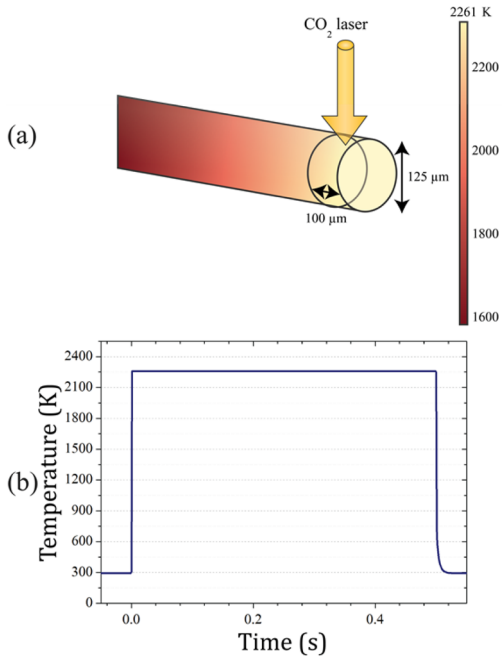

Fig. 1. Simulation model of laser-based heating: color map (a) illustrating heat distribution in the fiber during CO_2 laser exposure and (b) temperature profile of the silica fiber tip exposed to 0.5 s CO_2 laser pulse.

Table 1. Powder Mixture Used in Our Experiments

	Er_2O_3	Al_2O_3	SiO_2
Composition	0.7 wt%	5.7 wt%	93.6 wt%
Particle size	≤100 nm	13 nm	15 nm
Purity	99.9%	99.8%	99.8%

Figure 2 depicts the experimental setup used for sample investigation. To simulate typical temperatures used in any glassmaking processes, the samples were heated to their softening point using a focused CO_2 laser beam ($\lambda = 10.6\,\mu m$, $P = 4\,W$, spot size of 120 μm). To target the early dynamics of glassmaking, and Er^{3+} clustering, samples were subjected to elevated temperatures for intervals ranging from 0.5 s to 128 min (see Fig. 3(a)). In each interval, the samples were cooled to room temperature, and the fluorescence lifetime (τ) was probed. Here, the samples were excited with 976 nm diode laser (power of 3 W, output fiber with a 50 μm and a 0.22 NA) and focused through two lenses ($f_1 = 30\,mm$; $f_2 = 45\,mm$). This process was repeated, making each heating interval represent the total accumulated heating time. During the experiments, the samples remained stationary, while each laser (CO_2 and laser diode, as shown in Fig. 2) was launched sequentially, ensuring consistent exposure parameters throughout. The pump power was experimentally optimized for a trade-off between high-energy effects and obtaining a well-to-be-measured signal, given possible beam misalignments. The rectangular pump pulses are 0.4 s long with a switch on and off time of 0.4 ms. The resulting spontaneous emission ($\lambda_s = 1550\,nm$) was monitored through the MMF using a fiber-coupled fast avalanche photodiode (APD) (bandwidth of 1 GHz) and oscilloscope (bandwidth of 1 GHz).

To filter the emission signal from the pump, a low-pass filter (Thorlabs FELH1000) was used. The decay of λ_s was fitted with an exponential function to estimate τ. It is important to note that the use of a pump beam with 0.4 ms fall time allows us to probe

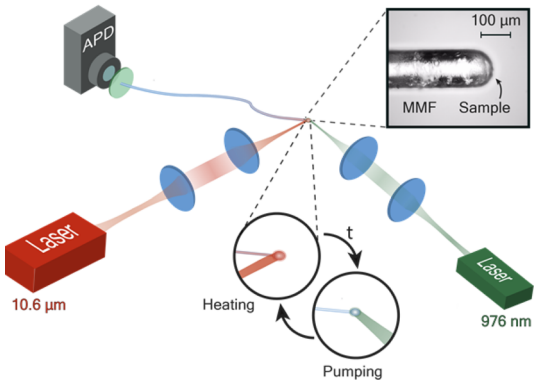

Fig. 2. Schematic of the experimental setup for sample investigation. The inset shows a typical micrograph of a laser-sintered Er^{3+}-doped sample.

only emissions with long (ms) lifetimes, which are typically associated with the ion interactions with the glass network. By carefully controlling heat exposure and dopant diffusion, we aim to maximize τ in highly doped samples, enabling a deeper understanding of the cluster dynamics.

In Fig. 3(a), the normalized τ values (relative to the maximum) for several heating intervals are presented. The trend shows a rapid increase in τ during the first few minutes of heat exposure, reaching its peak after 2 min of CO_2 laser irradiation. This behavior can be attributed to the gradual dissolution of Er_2O_3 powder into the aluminosilicate glass network, with initial low clustering. We have obtained a maximum lifetime of $\tau \approx 9.0 \pm 0.2$ ms in all investigated samples, which compares to other reported results in Er-doped fibers [15,19]. Following the 2 min threshold, the lifetime gradually decreased following a semi-exponential trend. This illustrates gradual cluster formation within the laser-sintered glass. It is evident that following 20 min heat exposure, the change is less rapid. This is in-line with the earlier studies, which showed minimal ion dynamics in the case of traditionally made fibers [15,16]. To rule out the dynamic change of hydroxyl (OH^-) groups that are known to have a major impact on obtained lifetimes [3], Raman microscopy analysis (WITec alpha300 R) was conducted at three stages of sample processing: post-sintering (0.5 s), 2 min, and 64 min, as indicated in Fig. 3(c), with corresponding markers in Fig. 3(a). The ratio between OH^- and silica Raman peaks appears to be consistent throughout the investigated range (±0.1%) (Fig. 3(c), inset). This suggests consistent OH^- content in the samples, which remains unaffected by laser heating. The spectral emission of the sample was evaluated *in situ* after cooling down with a spectrum analyzer, confirming the amplified spontaneous emission (ASE) characteristic for Er^{3+} doping (Fig. 3(b)). The thermal history had no observable impact on its spectrum. Noteworthy, due to low ASE strength inherently linked to our low-volume sample, the spectrum shown in Fig. 3(b) was integrated over a long time. To gain a deeper understanding into cluster formation, as well as to underline the role of alumina in the laser-sintered glass, we prepared laser-sintered samples of pure Er_2O_3 powder (ER100). Thus, following the initial sintering, a phase separation between silica glass and the sintered sample was visible (see inset in Fig. 4(a)). We observed a gradual lifetime increase in all heat-exposure intervals. In the first minutes, the lifetime sees a rapid surge coming from 75% of the maximal lifetime to 95% in a matter of several minutes as shown in Fig. 4(a). After

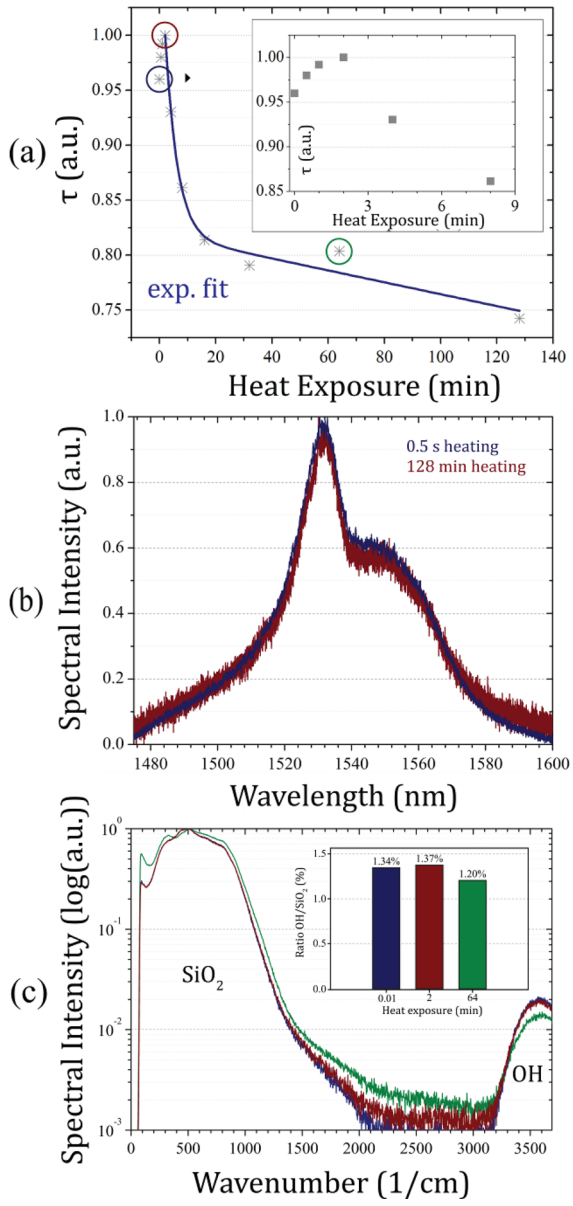

Fig. 3. (a) Normalized lifetime of laser-sintered glass samples for different heat-exposure intervals (starting with 0.5 s), (b) normalized emission spectrum of the laser-sintered sample after 0.5 s and 128 min heating, and (c) Raman shift of the laser-sintered samples. The inset shows the maximum ratio of OH^- compared to SiO_2.

around 30 min the increase becomes less rapid following the fit described in Eq. (2):

$$\tau(x) = 15.9\,(1 - e^{-(0.06(x-3.98))^{0.04}}), \quad \textbf{(2)}$$

where x is the heat exposure in minutes. This can be linked to gradual diffusion of Er^{3+} into MMF's glass network. Figure 4(b) shows a typically obtained signal at λ_s for the ER100 sample and for our laser-sintered alumino-silica samples as comparison. During pumping, in the pulse envelope of the ER100 sample, we observed gradually increasing signal strength, but none in the alumino-silica sample. The origin of this is likely twofold. In the first contribution, the expedited depopulation of UC levels, such as $^4F_{7/2}$, facilitates the population of the $^4I_{13/2}$ state, contributing to the gradual increase in fluorescence intensity. The second

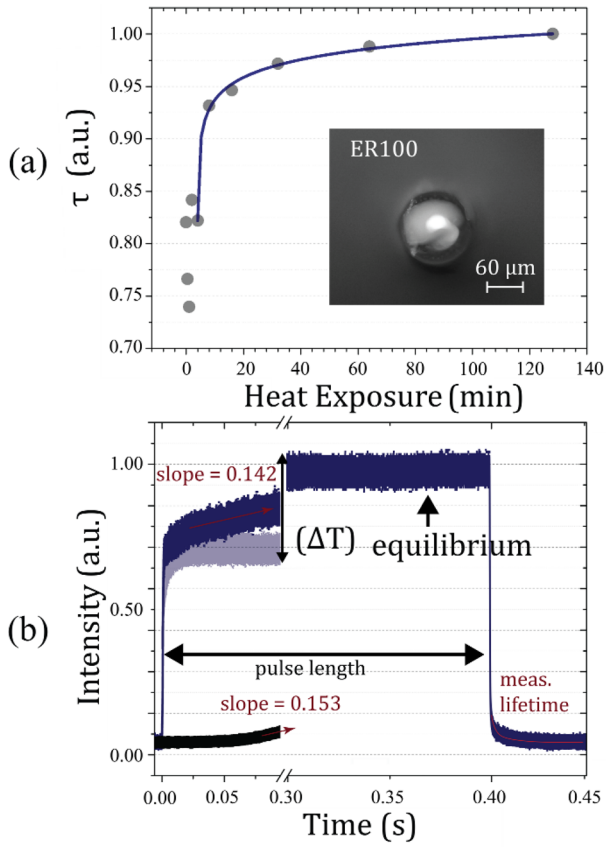

Fig. 4. (a) Normalized and fitted (see Eq. (2)) lifetime of laser-sintered samples with pure Er_2O_3 powder (alumino-silica powder sample in semi-transparent); the inset shows a typical top-view of the sample with visible phase separation (bright area) and (b) a typically obtained signal at λ_s (blue) as well as blackbody contribution of a carbon-coated fiber with high absorption and no fluorescence as comparison (black).

contribution can be linked to pump-originated heating. This was evident as the longer excitation pulses give the system a chance to reach an equilibrium of temperature, whereas shorter pulses make the system prone to rapid heating and thus thermal radiation influencing the obtained signal strength (marked with ΔT in Fig. 4(b)). To quantify the blackbody contribution, we used a carbon-coated fiber (CCF), which was designed to achieve high absorption at $\lambda_p = 980$ nm without fluorescence. The CCF was pumped under the same conditions as the ER100 sample (see Fig. 4(b) in black), demonstrating a comparable heat rate and emission. This highlights that thermal radiation is the dominant factor contributing to the increase of signal strength. Furthermore, the trends depicted in Fig. 4(b) indicate high clustering in samples without alumina, leading to processes such as parasitic upconversion (UC). UC results in a loss of excitation energy and non-radiative relaxation, which heats up the test sample.

In conclusion, we have shown that by controlled heat exposure, it is possible to maximize radiative lifetime, thus mitigating clustering in the laser-sintered glass. In our test samples, the maximum lifetime was obtained following approximately 2 min heating. Although such fabrication time may not be feasible for full specialty fiber manufacturing, it was shown that the most rapid performance decreases, i.e., 20% lifetime decrease can be linked to the first 30 min of high-temperature processing. These results highlight that rapid laser-based fabrication techniques may play a pivotal role in fabricating highly doped, high-gain RE-doped materials, as they enable fast and localized heating profiles that mitigate ion mobility and parasitic energy transfers.

Funding. European Research Council (101072409); Vetenskapsrådet (2022-06180).

Acknowledgment. The authors thank Prof. John Ballato for his valuable insights, constructive discussions, and assistance in the analysis of the results.

Disclosures. The authors declare no conflicts of interest.

Data availability. Data underlying Figs. 3 and 4 can be found in Dataset 1, Ref. [27].

REFERENCES

1. M. K. Hossain, S. Hossain, M. H. Ahmed, *et al.*, ACS Appl. Electron Mater. **3**, 3715 (2021).
2. M. N. Zervas and C. A. Codemard, IEEE J. Sel. Top. Quantum Electron. **20**, 219 (2014).
3. M. J. F. Digonnet, *Rare-Earth-Doped Fiber Lasers and Amplifiers* (Marcel Dekker, 2001).
4. P. Maniewski, T. J. Wörmann, V. Pasiskevicius, *et al.*, J. Am. Ceram. Soc. **107**, 5143 (2024).
5. W. Blanc, J. Ballato, and M. Ferrari, Eur. Phys. J. Plus **138**, 858 (2023).
6. J. Ballato, H. Ebendorff-Heidepriem, J. Zhao, *et al.*, Fibers **5**, 11 (2017).
7. R. G. Smith, Appl. Opt. **11**, 2489 (1972).
8. J. O. White, A. Vasilyev, J. P. Cahill, *et al.*, Opt. Express **20**, 15872 (2012).
9. M. M. Bubnov, V. N. Vechkanov, A. N. Gur'yanov, *et al.*, Inorg. Mater. **45**, 444 (2009).
10. W. A. Pisarski, J. Pisarska, R. Lisiecki, *et al.*, Opto-Electron. Rev. **25**, 238 (2017).
11. J. Campbell, M. A. Cahoon, M. Gachich, *et al.*, Opt. Lett. **49**, 6721 (2024).
12. R. S. Quimby, W. J. Miniscalco, and B. Thompson, J. Appl. Phys. **76**, 4472 (1994).
13. L. D. Iskhakova, F. O. Milovich, M. E. Likhachev, *et al.*, J. Non-Cryst. Solids **554**, 120616 (2021).
14. K. Lyytikäinen, S. T. Huntington, A. L. G. Carter, *et al.*, Opt. Express **12**, 972 (2004).
15. P. Vařák, M. Kamrádek, J. Aubrecht, *et al.*, Opt. Mater. Express **14**, 1048 (2024).
16. P. Vařák, I. Kašík, P. Peterka, *et al.*, Opt. Express **30**, 10050 (2022).
17. K. Dybdal, N. Bjerre, J. E. Pedersen, *et al.*, SPIE Fiber Laser Sources and Amplifiers **1171**, 209 (1990).
18. P. Maniewski, A. I. Flint, R. H. S. Bannerman, *et al.*, APL Photonics **9**, 111301 (2024).
19. P. Maniewski, M. Brunzell, L. Barrett, *et al.*, Optica **10**, 1280 (2023).
20. D. Blaser, P. Hänzi, S. Pilz, *et al.*, Fibers **11**, 95 (2023).
21. B. Zheng, J. Yang, F. Qi, *et al.*, J. Non-Cryst. Solids **573**, 121129 (2021).
22. M.-H. Lai, K.-S. Lim, D. S. Gunawardena, *et al.*, IEEE Sens. J. **17**, 2961 (2017).
23. P. Maniewski, C. M. Harvey, K. Mühlberger, *et al.*, Opt. Mater. Express **12**, 2426 (2022).
24. J. M. Jones, P. E. Mason, and A. Williams, J. Energy Inst. **92**, 523 (2019).
25. C. M. Harvey, K. Mühlberger, T. Oriekhov, *et al.*, J. Opt. Soc. Am. B **38**, F122 (2021).
26. A. D. McLachlan and F. P. Meyer, Appl. Opt. **26**, 1728 (1987).
27. T. Wörmann, "Er^{3+}-doped silica glass lifetimes and spectra," Zenodo (2025) [retrieved 30 May 2025], https://doi.org/10.5281/zenodo.15336393.